Exploration of satellite-derived data products for atmospheric turbulence studies

Derek J Griffith*[a], Arshath Ramkilowan[a], Detlev Sprung[b], Erik Sucher[b], Cornelius J Willers[a], Gert J R Coetzee[c], Ryno van Staden[a]
[a]Optronic Sensor Systems (OSS), Council for Scientific and Industrial Research (CSIR), P O Box 395, Pretoria 0001, South Africa
[b]Fraunhofer Institute of Optronics, System Technologies and Image Exploitation (IOSB), Gutleuthausstraße 1, 76275 Ettlingen, Germany
[c]South African Weather Service (SAWS), Rigel Avenue South 442, Erasmusrand, Pretoria, South Africa

ABSTRACT

The quality, availability and diversity of satellite-derived earth observation data products are continuously improving. Such satellite products can provide an extensive and complementary view on many matters with respect to intensive but localised in-situ or ground measurements. A search has been undertaken on the available types and sources of satellite data products that could be applicable in the study of the spatio-temporal distribution of aero-optical turbulence in the atmospheric boundary layer. This has included all satellite data products that are relevant to the surface energy balance such as surface reflectance, temperature and emissivity. It was also important to identify active archive data services that can provide pre-processed and quality-filtered time-series products. Products derived from the Moderate Resolution Imaging Spectrometer (MODIS) and other sensors on the NASA Terra and Aqua platforms were of special interest. The use of climatological shortwave and longwave radiative transfer models, combined with satellite-derived data was explored as a method of elucidating the surface heat balance. An in-situ dataset from the Rietvlei vertical turbulence profiling campaign of 2013 was used to validate a number of aspects of the satellite-derived heat balance approach.

Keywords: Atmospheric turbulence, surface heat balance, satellite data products

1. INTRODUCTION

Optical surveillance along sightlines through the Atmospheric Boundary Layer (ABL) is limited chiefly by turbulence, aerosols and clouds. Reliable optical range performance predictions in a specific environment require data and models of these aspects and the phenomena which drive them. Turbulence, mainly related to air temperature fluctuations, is particularly problematic for long-range optical surveillance in daytime scenarios. The strength, spatial distribution and evolution of thermally-driven turbulence in the ABL is a complex picture driven by radiative transfer, terrain, local weather conditions and weather history as well as surface cover.

Surveillance from airborne and other elevated platforms is of growing interest and optimal configuration and deployment of such assets is an important consideration. Design and strategic configuration of elevated surveillance systems can benefit from statistical models of ABL state and the expected effect on optical surveillance in the deployment theatre. Tactical configuration and deployment of optical surveillance assets can benefit from realtime synoptic views of ABL state and the expected effect on optical range.

Data products derived from satellite Earth Observation (EO) systems can help to address both strategic and tactical optimisation of optical surveillance system configuration and deployment. EO data products are continuously improving in terms of quality, diversity and availability. Of particular interest is the relatively recent debut of powerful active EO data product archives that can produce summary, time series and synergistic views derived from very large EO datasets. These higher level data views would be very challenging or impossible to produce using average client-side resources.

In this work, we undertook to investigate some of the satellite data product and server-side processing resources that are currently available and that could be used for the above purposes, with particular attention to the problem of thermally-driven atmospheric turbulence.

*dgriffith@csir.co.za; phone +27 12 841 3371; fax +27 12 841 4015; www.csir.co.za

Some validation of satellite EO derived datasets was performed using in-situ data obtained during the Rietvlei trial executed in June 2013[1] .

2. SURFACE ENERGY BALANCE

A simple, one-dimensional model for the surface energy balance at the base of an idealised ABL is provided by[2]

$$E_N = E^{\downarrow} - E^{\uparrow} = H + H_L + H_G, \tag{1}$$

where $E^{\uparrow}$ is the total upwelling radiative flux (irradiance), $E^{\downarrow}$ is the total downwelling irradiance, H_L is the upward latent energy flux per unit area, H is the sensible heat flux (positive upward) per unit area and H_G is the ground heat flux (or "soil" heat flux, positive upward) per unit area. All quantities are in units of W/m^2. The latent energy is carried mostly by water vapour evaporated or emitted by vegetation through transpiration at the surface (together referred to as evapotranspiration), or by dew and frost formation when negative. The difference between the upwelling and downwelling irradiance, $E_N = E^{\downarrow} - E^{\uparrow}$ is the net downward radiative flux or irradiance.

The total upward and downward fluxes can each be separated into solar shortwave and thermal longwave components as

$$E^{\uparrow} = E_S^{\uparrow} + E_L^{\uparrow} \tag{2}$$

$$E^{\downarrow} = E_S^{\downarrow} + E_L^{\downarrow}. \tag{3}$$

The upward and downward shortwave fluxes are related through the effective surface albedo ρ, whereas the surface emissivity ε, together with surface absolute temperature T determines the emitted thermal flux from the surface ($\varepsilon\sigma T^4$ according to the Stefan-Boltzman law) as well as the reflected component of the downwelling thermal flux. Hence,

$$E_N = E_S^{\downarrow} - E_S^{\uparrow} + E_L^{\downarrow} - E_L^{\uparrow} \tag{4}$$

$$= E_S^{\downarrow} - \rho E_S^{\downarrow} + E_L^{\downarrow} - \left[(1-\varepsilon)E_L^{\downarrow} + \varepsilon\sigma T^4\right] \tag{5}$$

$$= (1-\rho)E_s^{\downarrow} + \varepsilon(E_L^{\downarrow} - \sigma T^4), \tag{6}$$

where σ is the Stefan-Boltzmann constant.

In reality, the effective albedo ρ is dependent on the spectral distribution as well as the angular distribution of the downward radiative flux. The emissivity ε is generally also wavelength dependent. Mindful of these and other complexities such as angular dependence of reflectance, estimates of the surface albedo and emissivity, for example, can be obtained from readily available satellite data products, discussed below.

2.1 Sensible Heat Flux

The sensible heat flux H is the major direct driver in the development of the convective boundary layer during the day and hence also the development of thermal turbulence affecting optical imaging[3] . Sensible heat flux can be measured in several ways, including Eddy Covariance (EC), scintillometry and sonic anemometry. The latter two methods were utilised at the Rietvlei campaign[1] .

2.2 Upwelling and Downwelling Irradiance

Total upwelling irradiance $E^{\uparrow}$ and downwelling irradiance $E^{\downarrow}$ can be measured with suitable radiometers. For the shortwave flux, upward and downward-facing pyranometers are the typical configuration, while a pyrgeometer is used to measure the longwave thermal component. At the Rietvlei campaign two instruments were used, one providing downwelling shortwave flux (Delta-T Devices® model SPN1), differentiated into total (or global) and diffuse horizontal components, while a pyrgeometer was deployed for the longwave component. The shortwave radiometer was only operated in the downwelling mode, while the pyrgeometer was operated looking upwards for approximately half of the campaign and downwards for the remainder. Radiative fluxes can also be calculated with a Radiative Transfer Code (RTC) if the surface spectral reflectance, temperature and emissivity are known together with sufficient atmospheric state information. The libRadtran suite[4] was used to compute radiative fluxes.

3. SATELLITE EO DATA PRODUCT SOURCES

Remote sensing of surface energy fluxes and soil moisture levels have become major fields of expertise[5] . Here, we focus on more accessible sources of satellite-derived data products.

3.1 NASA Giovanni

The Giovanni platform is a web-based (http://disc.sci.gsfc.nasa.gov/giovanni) service offered by NASA Goddard Earth Sciences, Data and Information Services Center (GES DISC). Giovanni comprises a number of portals to various application domains for earth science data, much of which is satellite-derived or hybrid satellite/in-situ product. Under the class of meteorological portals, 2D and 3D hourly data can be obtained from the Modern Era Retrospective Analysis for Research and Applications (MERRA) portal. MERRA 2D hourly data is available for sensible (H) and latent (H_L) heat flux. The MERRA sensible heat flux hourly values can be compared to the in-situ measurements at Rietvlei from the sonic anemometer data. Vertical profiles of temperature, water vapour and ozone, amongst others are available on a 3-hourly time grid from the MERRA 3D portal. These profiles can be compared to radiosonde data, if available.

There are numerous other products available through the Giovanni platform of general interest to surveillance applications including Aerosol Optical Thickness (AOT) at various wavelengths as well as other aerosol properties, wind, cloud parameters including optical thickness and surface reflectance.

The AeroStat Giovanni portal (http://giovanni.gsfc.nasa.gov/aerostat/) offers statistical analysis, visualization and downloadable products from aerosol data measured by satellites and ground-based Aeronet (http://aeronet.gsfc.nasa.gov/) stations.

Aerosol and cloud data are of relevance since these factors are major modulators of the solar radiation reaching the surface, which in turn is a major driver of thermal turbulence.

Under the class of Giovanni hydrology portals, the Global Land Data Assimilation System (GLDAS) provides 3-hourly surface parameters on a 0.25° grid, including turbulent heat fluxes, ground heat flux (H_G), evapotranspiration, long and shortwave incident and net radiation as well as soil moisture. These parameters are derived from the Noah model.

According to the Giovanni website, some services are offered through the Simple Object Access Protocol (SOAP). This would allow for programmatic retrieval of these Giovanni products and services.

3.1.1 MERRA and SHADOZ

The Irene weather station in Pretoria, a facility of the South African Weather Service (SAWS), lies 8 km to the west of the Rietvlei reserve campaign area and at the same altitude. Conventional (InterMet®) radiosondes are released from Irene at around midday. Irene is also an active site in the Southern Hemisphere Additional Ozonesondes (SHADOZ - http://croc.gsfc.nasa.gov/shadoz/) project[6] . Two SHADOZ ozonesondes were released from Irene during the Rietvlei campaign being at 2013-06-19 08:08 UTC and 2013-06-26 08:20 UTC. The temperature and relative humidity profiles from these two SHADOZ sondes were compared to profiles obtained through Giovanni/MERRA 3D. A comparison of the temperature profiles is shown in Figure 1. MERRA does not resolve the temperature inversion seen on 2013-06-19 in as much detail as the radiosonde. The US Air force Geophysical Laboratory (AFGL) temperature profiles for the mid-latitude summer and winter models are also plotted as a reference. The Rietvlei campaign environment would classify as sub-tropical winter and the AFGL mid-latitude summer profile is clearly a better fit.

A comparison of specific humidity profiles from SHADOZ and MERRA is shown in Figure 2. The surface relative humidity from MERRA and SHADOZ as well as the measured in-situ relative humidities for a number of test points are shown in Table 1.

Some of the differences in Figures 1 and 2 are explained by the difference in effective spatial and temporal sampling patterns of the MERRA and SHADOZ results. The MERRA surface relative humidity is reasonably consistent with in-situ measurements.

The sensitivity of the computed surface radiative fluxes due to the differences seen in Figure 2 are investigated and reported below.

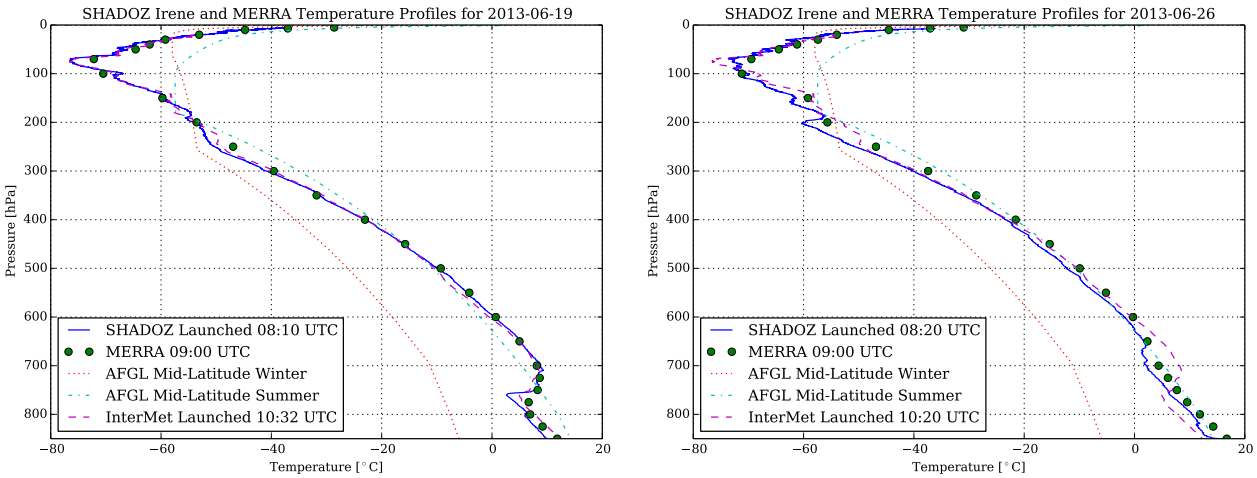

Figure 1. Temperature Profiles from SHADOZ (Irene) and MERRA (Rietvlei), 2013-06-19 (left) and 2013-06-26 (right)

Table 1. Surface Relative Humidity, SHADOZ, MERRA, InterMet and In-Situ

Date	Time (UTC)	SHADOZ	MERRA	InterMet	Rietvlei In-Situ
2013-06-19	08:10	62.0%			51.8%
2013-06-19	09:00		44.4%		44.6%
2013-06-19	10:32			41.0%	38.0%
2013-06-26	08:20	35.0%			33.6%
2013-06-26	09:00		24.4%		32.3%
2013-06-26	10:20			26.0%	26.8%

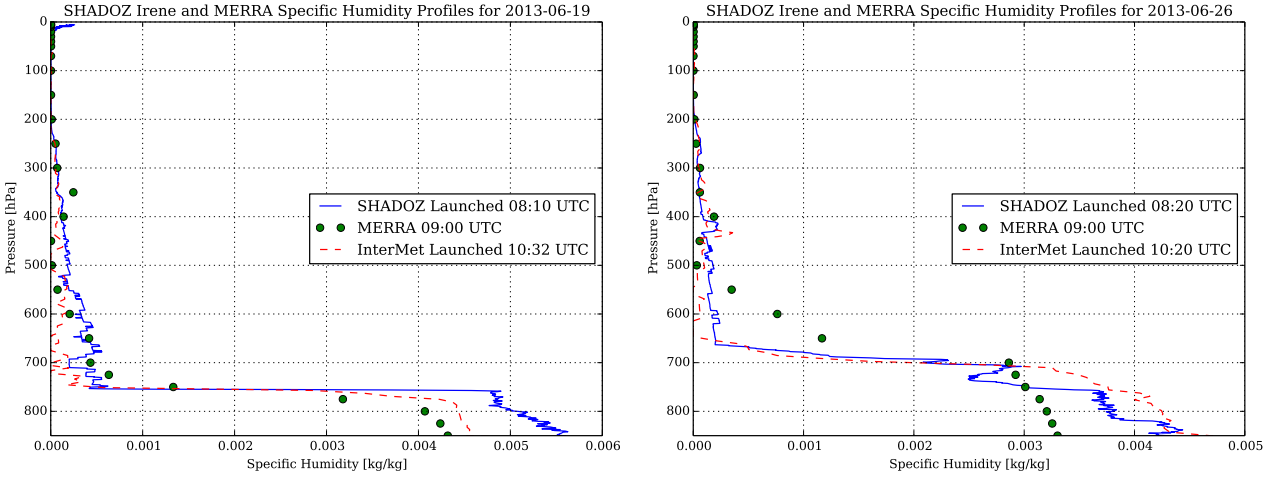

Figure 2. Specific Humidity Profiles from SHADOZ (Irene) and MERRA (Rietvlei), 2013-06-19 (left) and 2013-06-26 (right)

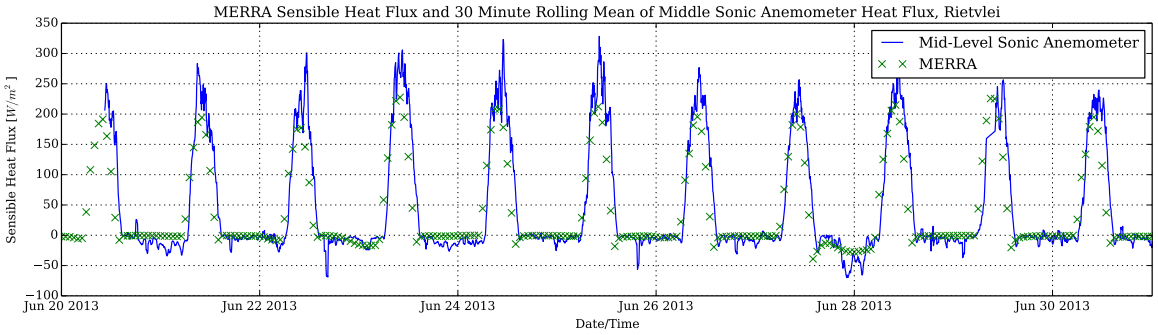

Figure 3. Comparison of Giovanni/MERRA Sensible Heat Flux with Sonic-Anemometer In-situ Sensible Heat Flux

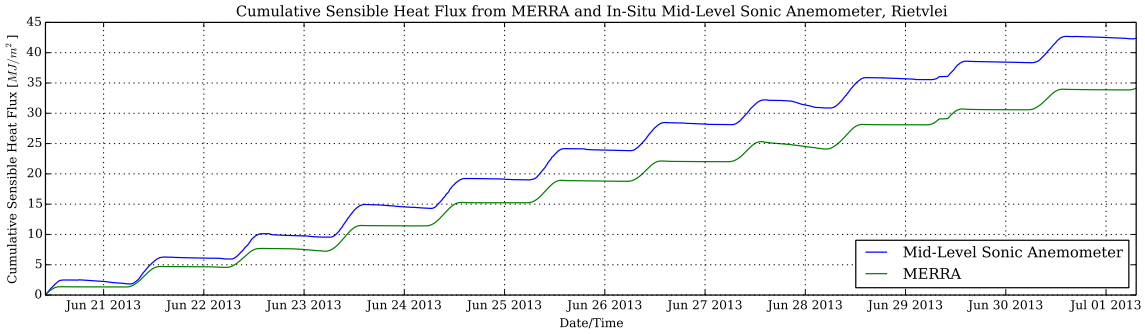

Figure 4. Comparison of Giovanni/MERRA Cumulative Sensible Heat Flux with Sonic Anemometer Cumulative Sensible Heat Flux

3.1.2 MERRA Sensible Heat Flux

An hourly time-series for sensible heat flux (H) and latent heat flux (H_L) at Rietvlei was extracted through the Giovanni/MERRA portal for the duration of the campaign (2013-06-18 to 2013-07-01). This was compared to sensible heat flux derived from the sonic anemometer data recorded at Rietvlei. The result for the comparison with the middle sonic anemometer (10.2 m above ground level) smoothed with a rolling mean over 30 minutes, is shown in Figure 3.

The MERRA data obviously does not show the temporal detail provided by the in-situ sonic anemometer measurements and appears to underestimate the cumulative sensible heat flux, plotted in Figure 4. However, in this case it is clear that the MERRA estimates could serve as a reasonable proxy in the absence of in-situ measurements.

3.2 ORNL DAAC

The Oak Ridge National Laboratory (ORNL) Distributed Active Archive Center (DAAC) provides a global subsetting and time-series derivation for Moderate Resolution Imaging Spectrometer (MODIS) data from the NASA Terra and Aqua satellite platforms. The products available for subsetting and time-series generation from the ORNL DAAC are given in Table 2.

Moreover, this MODIS facility is available programmatically using the Simple Object Access Protocol (SOAP). The SOAP interface is entitled the ORNL DAAC MODIS Web Service. Example clients written in a number of different languages (including Python, Matlab and R) are available on the MODIS Web Service page. While Giovanni generally produces times-series results online fairly quickly, the web interface of the MODIS Global Subsets: Data Subsetting and Visualization facility produces a batch job that can take several days to complete depending on the job size and demand for the service.

Full details of the processing of MODIS reflectance, temperature and emissivity extractions for the Rietvlei area are available online in the form of an IPython notebook[7] .

Table 2. ORNL DAAC MODIS Global Subsets: Data Subsetting and Visualization Products

Product Code	Product Description
MCD43A1	MODIS/Terra+Aqua BRDF and Calculated Albedo
MCD43A4	MODIS/Terra+Aqua Nadir BRDF-Adjusted Reflectance 16-Day L3 Global 500m SIN Grid
MOD09A1	Surface Reflectance (Terra)
MOD11A2	Land Surface Temperature and Emissivity
MOD13Q1	Vegetation Indices (NDVI, EVI)
MOD15A2	Leaf Area Index (LAI) and Fraction of Photosynthetically Active Radiation (FPAR) 8 Day Composite
MOD17A2	Gross Primary Production (GPP)
MOD16A2	Evapotranspiration
MOD17A3	Net Primary Productivity (NPP)
MYD09A1	Surface Reflectance (Aqua)
MYD11A2	Land Surface Temperature/Emissivity
MYD13Q1	Vegetation Indices (NDVI, EVI)
MYD15A2	Leaf Area Index (LAI) and Fraction of Photosynthetically Active Radiation (FPAR) 8 Day Composite

3.3 SMOS

The amount of moisture in the soil and vegetation available for evapotranspiration influences the latent heat flux and therefore also the sensible heat flux. Besides soil type, the soil moisture level also influences the heat capacity and thermal conductivity of the soil and therefore the soil heat flux. In addition, soil moisture level in less vegetated (typically more arid) areas influences the solar spectrum reflectivity of the surface. Soil moisture is therefore a very important factor in the surface energy balance and development of the convective ABL[8] . The Soil Moisture and Ocean Salinity (SMOS) is a mission of the European Space Agency (ESA) that provides measurements of water content in the soil down to a depth of 1-2 m every 3 days at a lateral spatial resolution of 50 km. The sensor (MIRAS) is a passive aperture synthesis microwave system operating in the L-band at around 1.4 GHz. Currently there appears to be no data facility that produces SMOS time-series, and the spatial resolution is perhaps too low to provide a reliable measurement of soil moisture at the Rietvlei campaign area, which is dominated by urban land use on a scale of 50 km. However, the SMOS soil moisture product is potentially of interest when studying larger areas for statistical purposes.

Soil moisture products from SMOS are level 3 products available from Centre Aval de Traitement des Données SMOS (CATDS) at http://www.catds.fr/ on application. Results are typically in the NetCDF format. SMOS products could be used to help validate the Giovanni/GLDAS Noah modeled soil moisture products referred to in §3.1.

3.4 NASA Simple Subset Wizard

The NASA Simple Subset Wizard (SSW) at http://disc.sci.gsfc.nasa.gov/SSW/, provides a simple interface for spatial and temporal subsetting of a number of EO data products of potential relevance to the surface energy balance. The SSW is an alternative to Giovanni for MERRA and GLDAS products, but does processing offline and informs the user by email when the extraction has been completed (similar user model to the ORNL DAAC MODIS Global Subset service discussed above).

3.5 Other Sources

Many online satellite data order/delivery services do not offer time-series generation or spatial subsetting. In these cases it is generally necessary for the user to download data product “tiles” or “scenes” of fixed size, from which the relevant geographical subset must be extracted. This often involves downloading and processing of substantial amounts of data, much of which may be of no interest for point validation. However, this is certainly an option if the user has the required resources, in particular when performing validation with reference to in-situ measurements at a local campaign of short duration (such as the Rietvlei campaign) or when performing climatological studies over large areas. Examples of online services which offer this kind of dataset include the following:

- USGS Global Visualization Viewer (GloVis) - http://glovis.usgs.gov/
- NOAA Comprehensive Large Array - Data Stewardship System (CLASS) - http://www.class.ncdc.noaa.gov/
- NASA Reverb | ECHO - http://reverb.echo.nasa.gov/
- The ESA Earthnet Service - https://earth.esa.int/
- The ICARE Data and Service Centre at University Lille - http://www.icare.univ-lille1.fr/
- The World Data Centre for Remote Sensing of the Atmosphere (WDC-RSAT) - https://wdc.dlr.de/ and other data centres of the Global Atmosphere Watch (GAW)
- EUMETSAT - http://www.eumetsat.int/ and Satellite Application Facilities (SAF)

An extensive list of services for satellite data access can be found on the NASA Earth Observing System Data and Information System (EOSDIS) website at https://earthdata.nasa.gov/ under Search and Order Tools and the EOSDIS Data Service Directory.

The upcoming launch of the ESA Copernicus Sentinel 2 and 3 missions should bring a large and accessible satellite data product stream into play.

4. RADIATIVE TRANSFER COMPUTATIONS

The libRadtran RTC suite[4] was used to compute surface radiative fluxes (irradiances) and to analyse the sensitivity of radiative flux to various factors. The ideal was to reproduce measured (Reitvlei campaign) shortwave and longwave radiative fluxes at the surface, preferably only with satellite-derived inputs. Net shortwave (solar spectrum) and longwave (thermal spectrum) fluxes were computed using satellite-derived surface reflectance, temperature and emissivity as well as atmospheric state. To keep runtimes down, shortwave and longwave correlated-k models were used. These are climatological atmospheric radiative transfer models by Kato *et al.*[9] and Fu and Liou[10] for the shortwave and longwave respectively.

4.1 Aerosol Optical Depth

The Aerosol Optical Depth (AOD) is an important factor for radiative transfer. The nearest in-situ measurements of AOD for the Rietvlei campaign was the Aeronet node at CSIR/DPSS, which is 18 km north of the Rietvlei campaign site. Aerosols in the region during the winter months are primarily from biomass (grass) fires, and AOD can show significant short-term temporal and spatial variability. Since the Aeronet node was a substantial distance from the Rietvlei site, we selected 2 days which showed moderate AOD variability as measured by Aeronet to use for this exercise. The days selected were 2013-06-21 (pyrgeometer looking up) and 2013-06-26 (pyrgeometer looking down).

4.2 Surface Reflectance and BRDF

The surface reflectance at the Rietvlei campaign area was sampled over an area of approximately $100\,m^2$ using an Analytical Spectral Devices (ASD) Fieldspec spectroradiometer with calibrated white reference panel. A foreoptic of 8° total field of view was used on the spectroradiometer. This measurement configuration is close to that of the nadir view Bidirectional Reflectance Factor (BRF), being the ratio of the nadir (upwelling) radiance from the surface to that of a 100%-reflecting lambertian reference, the latter being closely approximated by the white reference panel. This is different from the total effective albedo ρ or spectral albedo $\rho(\lambda)$, which is the ratio of upwelling to downwelling flux (irradiance). The BRF is only the same as the albedo in any given situation if both the surface and the reference are lambertian. The mean reflectance (BRF) is shown plotted in Figure 5 together with the MODIS MOD09A1 channel surface reflectance values from the ORNL DAAC service[11] . The MODIS MOD09A1 reflectance product is also not a surface albedo in the strict sense and closer to a surface BRF although not at nadir.

The RTC expects as input the spectral albedo and makes the assumption that the surface is lambertian by default. In the case of libRadtran, it is possible to specify a Bidirectional Reflectance Distribution Function (BRDF) for the surface. This can be specified using spectral Rahman-Pinty-Verstraete (RPV-model)[12] parameters or MODIS Algorithm for Modeling Bidirectional Reflectance Anisotropies of the Land Surface (AMBRALS) model[13] parameters provided in the MODIS MCD43A1 product.

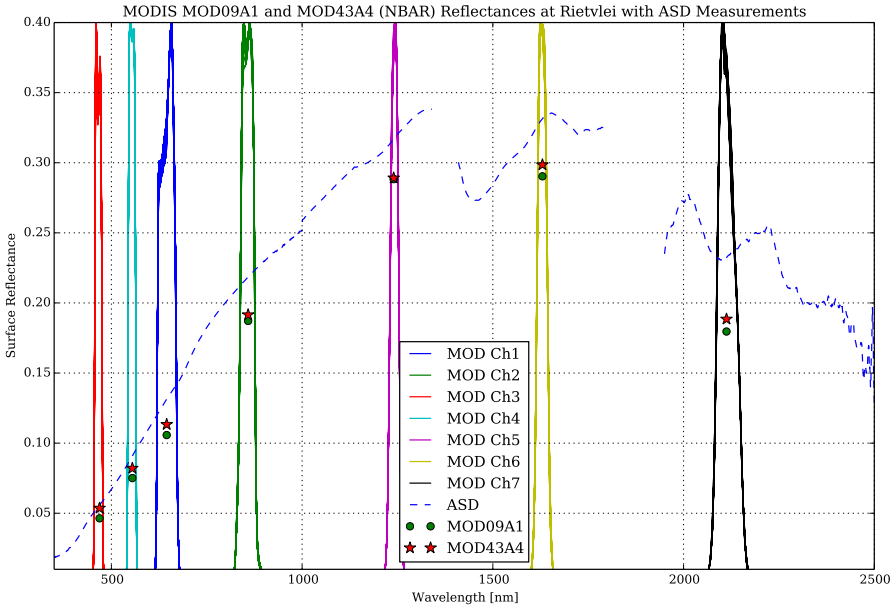

Figure 5. MODIS MOD09A1 and MOD43A4 Reflectances at Rietvlei, June 2013

RPV BRDF parameters are available from MISR satellite data products and are the preferred option as libRadtran accepts spectral variation of the RPV parameters. The MODIS MCD43A1 product together with computationally-estimated albedo is available from the ORNL DAAC. Use of this product in libRadtran is apparently difficult because only one set of AMBRALS parameters (single wavelength or fairly narrow band) can be entered per run. The MISR/RPV product does not appear to be available through active archives and would have to be extracted by the user.

The MODIS MOD43A4 product (see Table 2), also available through the ORNL DAAC MODIS subset service provides Nadir BRDF-Adjusted Reflectance (NBAR), which should be closer to the BRF measured with the ASD spectroradiometer, but the difference in this case is very small (see Figure 5). The difference between the ASD and MODIS reflectances is easily accounted for by the small spatial footprint of the ASD measurements compared to that of the MODIS subset time-series, which is on the order of several square kilometres.

The effect of non-lambertian surface BRDF has not been evaluated in this work, but is likely to introduce significant errors into the computation of radiative fluxes if not taken into account. This comment is more applicable to shortwave than to longwave flux computations although directional emissivity effects can also be significant in some cases (e.g. water targets).

4.2.1 GlobAlbedo

The GlobAlbedo project (http://www.globalbedo.org/) provides time-series for global albedo down to a scale of 1 km. As with the MODIS MCD43A1 product, mean albedo data is provided for broad bands in the visible, near-infrared and shortwave infrared spectral regions. The Directional-Hemispherical Reflectance (DHR) and Bi-Hemispherical Reflectance (BHR) albedo components are provided for each of the spectral regions, together with variances. The DHR is equivalent to the “black sky” albedo in the MODIS AMBRALS framework, while the BHR is equivalent to the MODIS “white sky” albedo.

4.3 Shortwave Surface Flux

Downwelling total and diffuse shortwave flux measured in-situ at Rietvlei on 2013-06-21 compared to RTC calculations (libRadtran/Kato) and GLDAS 3-hourly data are plotted in Figure 6. The upwelling shortwave flux was not measured in-situ at Rietvlei, so Figure 6 shows only the libRadtran/Kato and GLDAS upwelling shortwave flux.

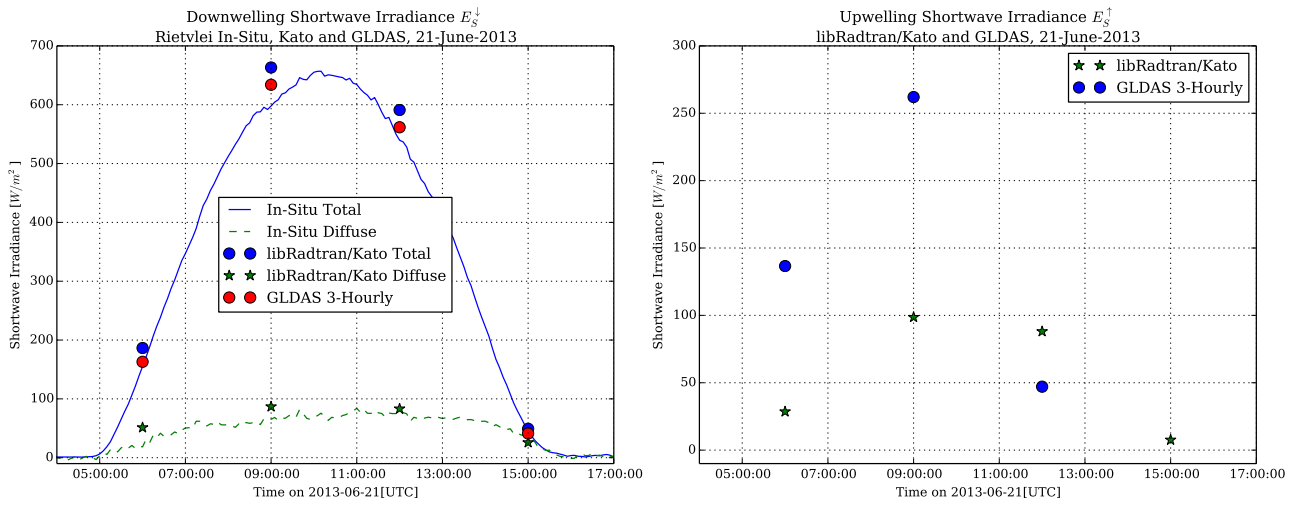

Figure 6. Downwelling and Upwelling Shortwave Flux, In-Situ, libRadtran/Kato and GLDAS 3-Hourly on 2013-06-21

Both libRadtran/Kato and GLDAS provide downwelling shortwave fluxes in this instance to within 10% of the measured flux. In the case of the upwelling shortwave flux, it is reasonable to conclude that GLDAS is overestimating this component for most of the day, since this would require unreasonably high effective surface albedo.

4.4 Temperature and Emissivity

Surface and near-surface temperatures for Rietvlei can be obtained from Giovanni/GLDAS on a 3-hourly basis and compared to in-situ data. In the RTC model, the surface temperature is set from the hourly MERRA "surface skin" data, which is a better fit to the in-situ measurements. The MERRA, GLDAS and in-situ data are plotted in Figure 7. The surface temperature is seen to be a fairly good match, but the GLDAS "near surface" air temperature is not a good match to in-situ data (see Figure 8). Satellite-derived time-series or snapshot data for air temperature at the surface appear to be difficult to obtain. There are empirical methods for estimating air temperature from Meteosat observations, for example[14] . Fortunately, air temperature is one parameter that is readily available from ground weather station networks which are generally ubiquitous.

Satellite data for the emissivity ε at Rietvlei was obtained both from MODIS and MERRA, which provide values of between 0.968 and 0.976 .

4.5 Longwave Surface Flux

Downwelling longwave flux measured in-situ at Rietvlei on 2013-06-21 compared to downwelling flux from the libRadtran/Fu and GLDAS 3-hourly product are shown in Figure 9. In the case of the libRadtran/Fu result, the total water vapour column had to be manipulated to get a good match to the measured flux. In fact, total water vapour column is available from several satellite-derived sources including Giovanni/MERRA 2D and this could be used as an input to the RTC. Surface temperature, relative humidity (from in-situ weather stations) and total water vapour column (satellite-derived) may serve as adequate inputs to the RTC to provide a reasonable estimate of downwelling longwave flux, but this is still to be verified against the Rietvlei dataset.

5. MONIN-OBUKHOV SIMILARITY THEORY (MOST)

Ultimately, the aim here was to determine the extent to which one can rely on freely available satellite derived products and if needed, typical weather station data to derive useful atmospheric turbulence statistics. Without the need for expensive equipment, together with the large spatial coverage and historical data profiles offered by satellite data, an attractive alternative for inferring turbulence statistics of the atmosphere is explored herein. The results were validated by sonic anemometer data captured during a field trial at the Rietvlei Nature Reserve[1] .

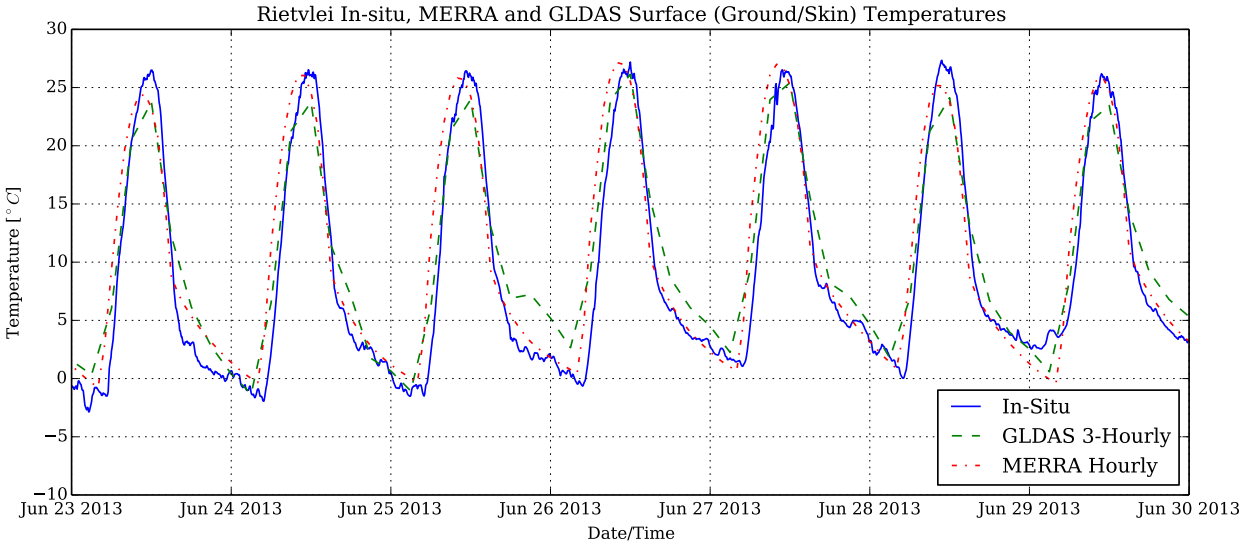

Figure 7. Comparison of Surface Temperatures at Rietvlei, In-Situ, MERRA and GLDAS

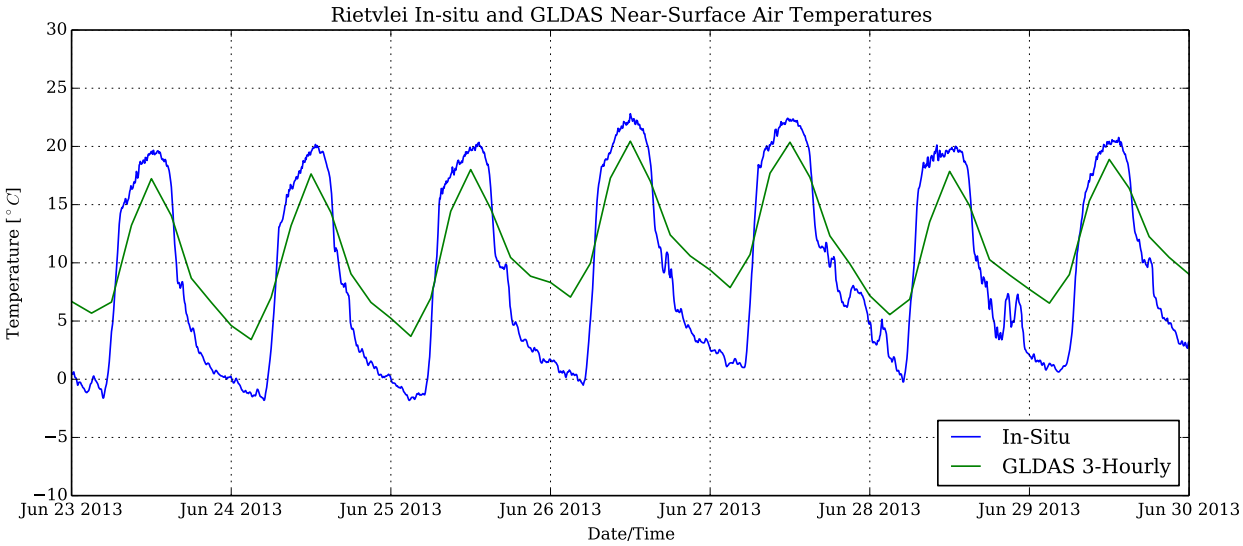

Figure 8. Comparison of Air Temperatures at Rietvlei, In-Situ and GLDAS

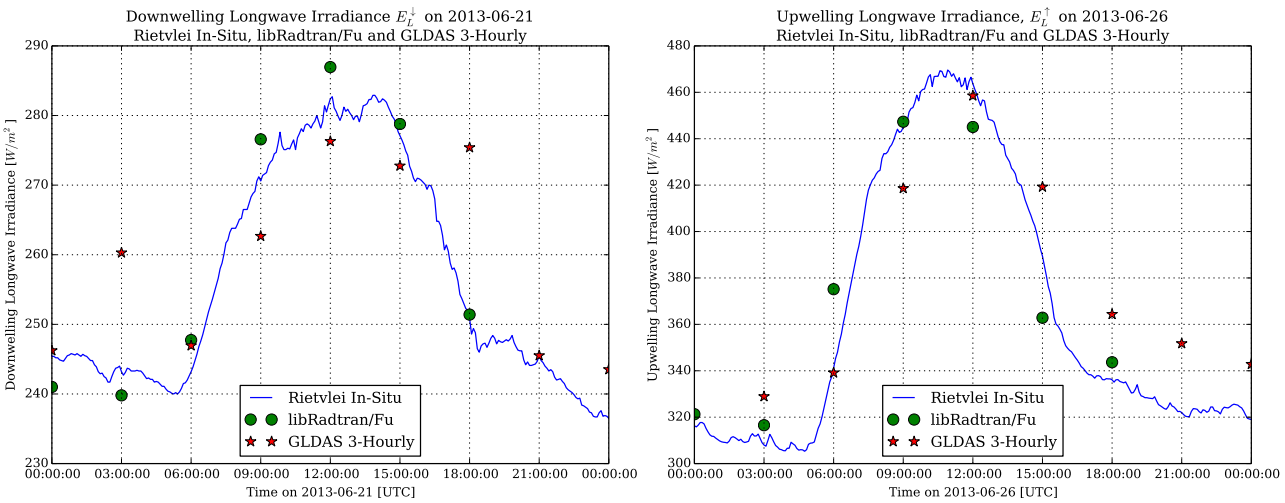

Figure 9. Downwelling and Upwelling Longwave Flux, In-Situ, libRadtran/Fu and GLDAS 3-Hourly

To ascertain the structure function parameter of refractive index, C_n^2, satellite derived data products and Monin-Obukhov Similarity Theory were utilised conjointly. In this instance, three hourly averages of sensible heat flux, and air temperature and wind speeds captured from MERRA were used. The defining equations of MOST are detailed below and can be used with confidence if the following conditions are met, as required by the similarity theory[15] :

- Steady state conditions
- Horizontal homogeneity of air flow
- Sufficiently developed turbulent fluxes that vary little with height

$$C_T^2 = T_*^2 z^{\frac{-2}{3}} f\left(\frac{z}{L_{MO}}\right) \tag{7}$$

Equation 7 is typically used to infer one of either sensible heat flux (H), or the spatial temperature structure parameter (C_T^2) provided the other is known. Here, T_* is the temperature scale (in degrees Kelvin), z is the height above ground at which the anemometer was stationed (in metres) and L_{MO} is the Obukhov length[16] . The factor $f\left(\frac{z}{L_{MO}}\right)$ is often referred to as a universal function, where the ratio within parenthesis is the dimensionless stability parameter. Several expressions for $f\left(\frac{z}{L_MO}\right)$ exist in the literature. The expressions considered herein have the following form and have been applied to only the unstable regime, where $\left(\frac{z}{L_{MO}}\right) < 0$,

$$f\left(\frac{z}{L_{MO}}\right) = CTT_1\left(1 - CTT_2\frac{z}{L_{MO}}\right)^{\frac{-2}{3}}. \tag{8}$$

Values for CTT_1 and CTT_2 are given in Table 3.

The friction velocity, u_* and the Obukhov length are co-dependent as can be seen from Equations 9 - 11. They are calculated in an iterative manner with the initial value for the friction velocity determined by exploiting the neutral conditions rule of similarity, which states that a universal function must be unity when it's stability parameter is zero. Three hourly temperature, wind and sensible heat flux averages where interpolated to five minute averages using in-situ sonic anemometer data. The anemometer was 4.6m above ground. A value of 0.4 for κ, the Von Karman constant was used for all calculations, unless otherwise required by a universal function. The roughness length z_0 was taken as 0.01m.[17]

$$L_{MO} = \frac{T u_*^2}{\kappa g T_*} \tag{9}$$

$$T_* = \frac{-H}{u_* \rho C_\rho} \tag{10}$$

$$u_* = uk[\ln \frac{z}{z_0} - \zeta(L_{MO})]^{-1} \tag{11}$$

$$\zeta(L_{MO}) = \begin{cases} \frac{-4.7z}{L_{MO}} & : \quad \frac{z}{L_{mo}} > 0 \text{ stable}, \\ 2\ln\left(\frac{1+y}{2}\right) + \ln\left(\frac{1+y^2}{2}\right) - 2\arctan(y) + \frac{\pi}{2} : & \quad \frac{z}{L_{MO}} < 0 \text{ unstable} \end{cases}$$

where $y = \left(\frac{1-15z}{L_{MO}}\right)^{\frac{1}{4}}$Assuming wavelength and humidity perturbations are negligible, the spatial structure function of refractive index can be determined using[16] Equation 12 below, where P is the air pressure in millibars.

$$C_n^2 = \left(79\frac{P}{T^2}10^{-6}\right)^2 C_T^2 \tag{12}$$

5.1 MOST Results

Figure 10 shows how the aforementioned MERRA data when applied to several universal functions (as listed in Table 3) compares to the in-situ sonic anemometer-derived C_n^2 .

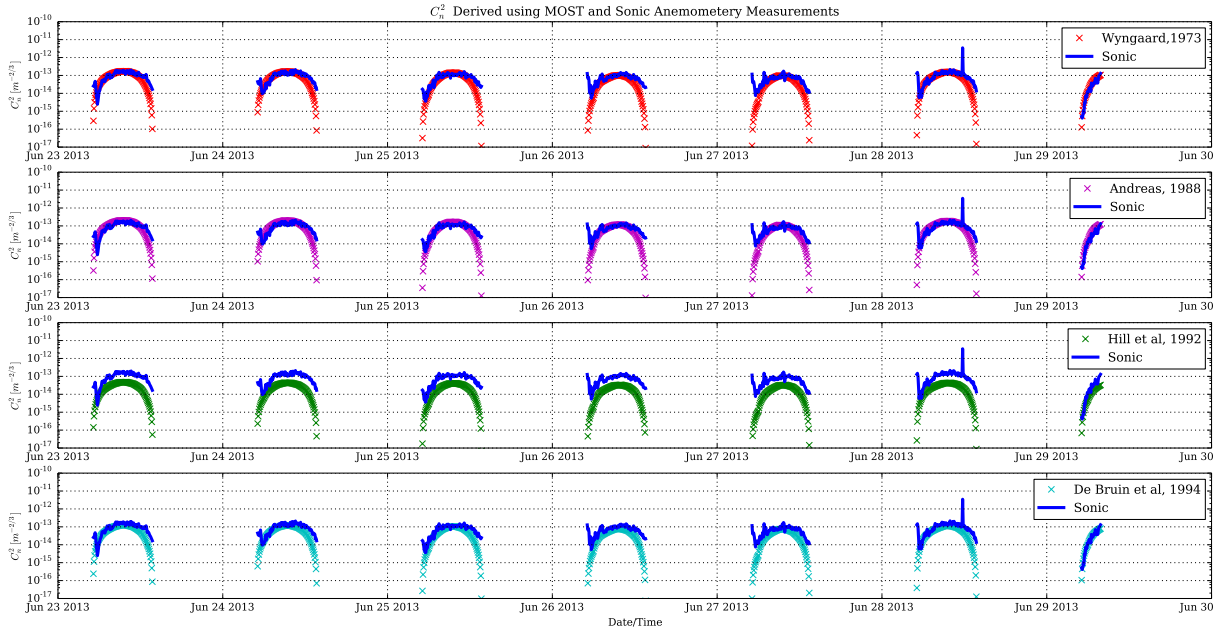

Figure 10. Comparison of C_n^2 from sonic anemometer and using MOST, during the Rietvlei campaign for unstable conditions

After excluding the obvious anomalies, the coefficient of determination of a linear regression was calculated for C_T^2 derived from sonic anemometry and MOST. This translates to an absolute percentage variation of C_n^2 measurements supplied in the adjacent column in Table 3. Values determined via the similarity theory were based on temperature,wind

Table 3. Regression of MOST Results

	CTT_1	CTT_2	$r_0^2(C_T^2)$	% error (C_n^2)
Wyngaard, 1973[18]	4.9	7	0.78	12.05
Andreas, 1988[19]	4.9	6.1	0.78	14.03
Hill *et al.*, 1992[20]	8.1	15	0.76	18.08
De Bruin, 1993[21]	4.9	9	0.77	10.59

and sensible heat flux measurements having a much coarser sampling resolution, as a result, the models were not able to accurately predict fluctuations on a finer time scale. The percentage errors, while implying a relatively modest absolute variation in C_n^2, Figure 10 suggests that the use of satellite-borne data and MOST to determine C_n^2 works in a reliable, predictable manner and can be used with relative confidence in areas where validation data is not available, provided the conditions stipulated by MOST are adhered to.

6. CONCLUSIONS

If the the conditions that are stipulated by MOST are adhered to in all respects, an error in C_n^2 of 10-20 % is inherent in the theory[15] . Moreover, the models listed herein, with the exception of Hill *et al*.[20] are said to be within 20% of each other. With this in mind the ~15% error of the the in-situ measurements, show that it is feasible to use satellite derived data products to attain at the very least, order of magnitude estimations of atmospheric turbulence for an area meeting the stipulated conditions of MOST.

In many cases, the suitability and validity of the satellite-derived products in this application are difficult to assess and validation should be performed in selected environments by means of in-situ measurement campaigns such as the Rietvlei campaign.

In general, with some significant limitations, satellite-derived data products available from active archives are a promising source of data for climatological assessment of surface and boundary layer thermal turbulence affecting electro-optical surveillance. One limitation is that the satellite-derived products are typically available on time scales of 1 to 3 hours or longer and do not have the spatio-temporal resolution associated with in-situ measurements. Short term variability of turbulence strength is an important consideration even in climatological studies. In-situ, time-intensive datasets will remain a key element in assessing suitability and validity of satellite-derived products in specific environments, and to provide information not obtainable from large coverage satellite or hybrid data sources.

For the purposes of optical surveillance through the ABL, the most useful sources of climatological time-series found in this study have been the NASA Giovanni platform and the ORNL DAAC MODIS Global Subset service. These services are a rich source of data on many ABL and surface state variables including cloud properties and amount, aerosol properties and amount as well as surface energy fluxes, reflectance and vertical profiles of temperature and humidity. The design of these platforms make such data much easier to access, particularly for those who are not specialists in satellite remote sensing products.

Follow-on work will comprise further investigation of available data products and determination of what is possible under cloudy conditions.

7. ACKNOWLEDGMENTS

Various analyses and visualizations used in this study were produced with the Giovanni online data system, developed and maintained by the NASA GES DISC at http://disc.sci.gsfc.nasa.gov/giovanni. We thank the SHADOZ project[6] for free data access.

REFERENCES

[1] Griffith, D. J., Sprung, D., Sucher, E., Ramkilowan, A., and Vhengani, L., "Comparison of slant-path scintillometry, sonic anemometry and high-speed videography for vertical profiling of turbulence in the atmospheric surface layer," *Proc. SPIE* **8890**, 889014–889014–10 (2013).

[2] Odhiambo, G. and Savage, M., "Surface layer scintillometry for estimating the sensible heat flux component of the surface energy balance," *South African Journal of Science* **105**, 208–216 (2009). http://dx.doi.org/10.4102/sajs.v105i5/6.92.

[3] Cheinet, S., Beljaars, A., Weiss-Wrana, K., and Hurtaud, Y., "The use of weather forecasts to characterise near-surface optical turbulence," *Boundary-Layer Meteorology* **138**(3), 453–473 (2011).

[4] Mayer, B., Kylling, A., Hamann, U., and Emde, C., *libRadtran, library for radiative transfer calculations* (December 2007). http://www.libradtran.org.

[5] Petropoulos, G., ed., [*Remote Sensing of Energy Fluxes and Soil Moisture Content*], Taylor & Francis (2013).

[6] Thompson, A. M., Witte, J. C., McPeters, R. D., Oltmans, S. J., Schmidlin, F. J., Logan, J. A., Fujiwara, M., Kirchhoff, V. W. J. H., Posny, F., Coetzee, G. J. R., Hoegger, B., Kawakami, S., Ogawa, T., Johnson, B. J., Vömel, H., and Labow, G., "Southern Hemisphere Additional Ozonesondes (SHADOZ) 1998-2000 tropical ozone climatology 1. Comparison with Total Ozone Mapping Spectrometer (TOMS) and ground-based measurements," *Journal of Geophysical Research: Atmospheres* **108**(D2) (2003).

[7] Cornelius J Willers, "Computational optical radiometry with pyradi," (2014). http://dx.doi.org/10.5281/zenodo.9910 and https://github.com/NelisW/ComputationalRadiometry.

[8] Pan, H.-L. and Mahrt, L., "Interaction between soil hydrology and boundary-layer development," *Boundary-Layer Meteorology* **38**(1-2), 185–202 (1987).

[9] Kato, S., Ackerman, T. P., Mather, J. H., and Clothiaux, E., "The k–distribution method and correlated–k approximation for a shortwave radiative transfer model," *J. Quant. Spectrosc. Radiat. Transfer* **62**, 109–121 (1999).

[10] Fu, Q. and Liou, K., "On the correlated k-distribution method for radiative transfer in nonhomogeneous atmospheres," *Journal of the Atmospheric Sciences* **49**(22), 2139–2156 (1992).

[11] Oak Ridge National Laboratory Distributed Active Archive Center (ORNL DAAC) (2014). MODIS subsetted land products, Collection 5, Available on-line from ORNL DAAC [http://daac.ornl.gov/MODIS/modis.html], Oak Ridge, Tennessee, U.S.A. Accessed August 17, 2014. Subset obtained for MOD09A1 product at 25.9115S,28.287E, time period: 2013-06-18 to 2013-06-26, and subset size: 2.5 x 2.5 km.

[12] Rahman, H., Pinty, B., and Verstraete, M. M., "Coupled surface-atmosphere reflectance (CSAR) Model 2 : Semiempirical surface model usable with NOAA advanced very high-resolution radiometer data," *Journal of Geophysical Research - Atmospheres* **98**, 20791–20801 (1993).

[13] Wanner, W., Strahler, A., Hu, B., Lewis, P., Muller, J.-P., Li, X., Schaaf, C., and Barnsley, M., "Global retrieval of bidirectional reflectance and albedo over land from EOS MODIS and MISR data: Theory and algorithm," *Journal of Geophysical Research: Atmospheres (1984–2012)* **102**(D14), 17143–17161 (1997).

[14] Cresswell, M. P., Morse, A. P., Thomson, M. C., and Connor, S. J., "Estimating surface air temperatures, from Meteosat land surface temperatures, using an empirical solar zenith angle model," *International Journal of Remote Sensing* **20**(6), 1125–1132 (1999). http://dx.doi.org/10.1080/014311699212885.

[15] Foken, T., "50 Years of the Monin-Obukhov Similarity Theory," *Boundary-Layer Meteorology* **119**, 431–447 (July 2006).

[16] Hutt, D. L., "Modeling and measurements of atmospheric optical turbulence over land," *Optical Engineering* **38**, 1288 (Aug. 1999). http://dx.doi.org/10.1117/1.602188.

[17] Hansen, F. V., "Surface Roughness lengths," Tech. Rep. August, U.S. Army Research Lab (1993).

[18] Wyngaard, J. C., "On Surface layer Turbulence," (Jan. 1983).

[19] Andreas, E. L., "Estimating Cn2 over snow and sea ice from meteorological data," *Optical Society of America* **5**(April 1988), 481–495 (1988).

[20] Hill, R. J., Ochs, G. R., and Wilson, J. J., "Surface-Layer Fluxes Measured Using the C_T^2 -Profile Method," *Journal of Atmospheric and Oceanic Technology* **9**, 526–537 (Oct. 1992).

[21] De Bruin, H. A. R., Kohsiek, W., and Van Den Hurk, B. J. J. M., "A verification of some methods to determine the fluxes of momentum, sensible heat, and water vapour using standard deviation and structure parameter of scalar meteorological quantities," *Boundary-Layer Meteorology* **63**, 231–257 (Mar. 1993).